ACS APPLIED MATERIALS & INTERFACES

Research Article

www.acsami.org

Clusters of Carbon Nanospheres Derived from Graphene Oxide

Sunatda Arayachukeat,[†,‡] Tanapat Palaga,[§] and Supason P. Wanichwecharungruang*[,⊥]

[†]Macromolecular Science Program, Faculty of Science, [‡]Center of Excellence on Petrochemical and Materials Technology, [§]Department of Microbiology, Faculty of Science, and [⊥]Department of Chemistry, Faculty of Science, Chulalongkorn University and Nanotec-CU Center of Excellence on Food and Agriculture, Bangkok 10330, Thailand

Supporting Information

ABSTRACT: Stable and water-dispersible cluster of carbon nanospheres (CCNs) can be synthesized from graphite or graphene nanoplatelets via sonication assisted chemical exfoliation/oxidation. Separation of CCNs with a diameter of ~130 nm from other products in the reaction including the graphene oxide sheets (GOShs) and other smaller carbon-based particles, could be done by centrifugation. Structural analysis of these CCNs by UV−vis absorption, fluorescent, IR, Raman, and X-ray photoelectron spectroscopic, combustion elemental, and electron diffraction analyses, indicates an extended $\pi-\pi$ conjugation network of sp^2-hybridized carbon atoms together with COOH, C═O, and OH functionalities. The spherical morphology of the CCNs is established by scanning electron microscopic analysis, while transmission electron microscopy indicates that the obtained CCNs are an aggregate of 5 nm carbon spheres (giant fullerenes) and GOShs. Dispersing the CCNs in curcumin solution results in curcumin adsorption onto the CCNs at 18.5 ± 1.4% (wt curcumin/wt loaded CCNs). The curcumin-loaded CCNs are taken up into human embryonic kidney (HEK293T) cells with detachment of the curcumin from the CCNs once inside the cells, such that curcumin is detected in the nucleus while the CCN carriers are only found outside the nucleus. The use of CCNs as the carrier gives a significantly better transportation of curcumin into the nucleus of the cells compared to curcumin alone. CCNs show no significant in vitro cytotoxicity to the HEK293T and human epidermoid cervical carcinoma cell lines at up to 3 μg/mL.

KEYWORDS: *graphene oxide, fullerene, curcumin, delivery, carbon*

INTRODUCTION

In the past 50 years, various carbon nanostructures, including spherical buckyballs or fullerenes,[1] giant fullerenes,[2,3] single-walled and multiwalled carbon nanotubes (SWCNTs and MWCNTs, respectively),[4] graphene sheets, graphene nanoribbons, carbon onions and cones,[5] and dahlialike and budlike aggregates,[6] have drawn considerable research interest. Their prospective applications as materials for various industries, such as multifunctional nanometer scaled catalytic, magnetic, and optoelectronic materials,[7−9] nanoelectronics,[10] polymer composites,[11] biosensors,[12] solar cells,[13] surfactants,[14] and gas absorption/storage,[15] have been pursued. Recently, many biomedical aspects of these various carbon nanostructures have been reported, including their cytotoxicity and biocompatibility,[16−18] and surface modifications for medical applications.[19,20] Their applications as biomaterials have been demonstrated in the areas of drug/gene delivery,[21−24] bone tissue engineering,[25,26] and cellular imaging.[27]

In 2009, Wang et al. demonstrated that sonicating GOShs in concentrated acids could cut them into nanofragments and soluble polyaromatics, which subsequently underwent cavitation-induced condensation to form various carbon nanostructures, including CNTs, fullerene-like carbon nanoparticles, and nanoribbons.[28] Transformation of one carbon nanostructure into other by both gas and solution phase processes have also been reported, including, for example, the transformation of graphene sheets into fullerenes,[29] GOShs into CNTs, and MWCNTs into nanoribbons.[30] Aggregation of small carbon nanostructures into larger morphologies, such as the aggregation of carbon nanohorns (20−50 nm in tubule length and 1−3 nm in diameter) into spherical particles of around 100 nm in diameter, and aggregation of C60 fullerenes into spherical particles of around 5−500 nm, has also been demonstrated in the gas phase.[31−33]

Indeed, noncovalent interactions can lead to the formation of graphitic carbon in various forms. Here, the in solution transformation of graphite and graphene nanoplatelets (GNPs) into a cluster of carbon nanospheres (CCN) is reported. Structural characterization of the CCN using various analytical techniques is reported, and the mechanism of formation of CCN is proposed. Finally, the application of the CCN as an efficient curcumin carrier is demonstrated in vitro.

EXPERIMENTAL SECTION

Materials. Natural flake graphite (graphite) of 200−300 μm in size was obtained from the Thai Carbon and Graphite Co., Ltd. (Bangkok, Thailand). Graphene nanoplatelets (GNPs) of 6−8 nm thick x 5 μm wide were purchased from Strem Chemicals, Inc. (Newburyport, MA,

Received: September 14, 2012
Accepted: November 26, 2012
Published: November 26, 2012

   dx.doi.org/10.1021/am3019959 | ACS Appl. Mater. Interfaces 2012, 4, 6808−6815

USA). Scanning electron microscopic (SEM) and transmission electron microscopic (TEM) images were obtained from JEOL JSM-6400 (using an accelerating voltage of 15 kV), and JEOL JEM-2100 (using an accelerating voltage of 120 kV in conjunction with selected area electron diffraction), respectively. The hydrated particle size, polydispersity index (PDI) and zeta potential were evaluated by dynamic light scattering (DLS) using a Malvern Zetasizer nanoseries model S4700 (using a He−Ne laser beam at 632.8 nm and scattering angle of 173°).

Scheme 1. Synthesis of CCNs from Graphite or Graphene Nanoplatelets (GNPs)

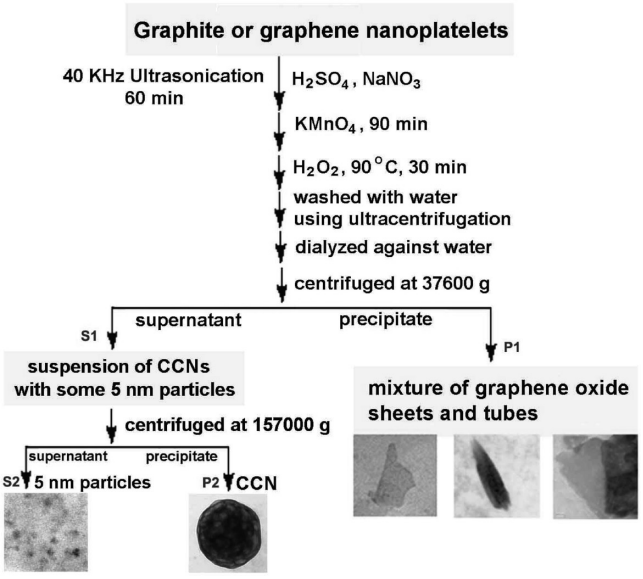

Synthesis of Cluster of Carbon Nanospheres (CCNs) (Scheme 1). One gram of graphite or GNP was mixed with 1.0 g of sodium nitrate and 50 mL of 18 M sulfuric acid and then sonicating the mixture at 40 kHz at room temperature for 1 h. Then, $KMnO_4$ (6.0 g) was added and the mixture was stirred for 90 min, followed by 100 mL of water and increasing the temperature to 90 °C for 30 min. After that, water (300 mL) was added, the mixture stirred for another 10 min and then the excess $KMnO_4$ was removed by adding 5% (w/v) H_2O_2 (50 mL) and stirring at room temperature for 30 min. Finally, the obtained mixture was dialyzed against water (CelluSep T4, MWCO of 12 000−14 000 Da, Membrane Filtration Products, USA), until pH 5−6 was reached. The oxidized carbon based materials of various morphologies, that were obtained at this stage were then centrifuged at 9,400 g for 10 min to precipitate various big sized precipitates, followed by centrifugation of the supernatant at 11,300 g for 15 min (to pellet the CNTs) and then at 21 100 g for 15 min (to pellet the GOShs). Finally, the supernatant was centrifuged at 37 000 g for 30 min to remove the residual smaller GOShs, leaving the supernatant containing the CCNs. The supernatant containing the CCNs was then ultracentrifuged at 157,000 g for 30 min to partially separate the CCNs from smaller particles (5 nm particles). The pelleted CCNs were then freeze-dried for storage and later resuspended in water by ultrasonication (40 kHz, 25 °C, 15 min) when required. Products were imaged by SEM and TEM. Chemical structure was evaluated by (i) UV−visible absorption spectroscopy (UV−vis, UV2500, Shimadzu), (ii) fluorescent spectroscopy (Varian Cary Eclipse fluorescence spectrophotometer), (iii) attenuated total reflectance-Fourier transform infrared spectroscopy (ATR-FTIR, Nicolet 6700), (iii) Raman spectroscopy (Thermo Electron Raman microscope, equipped with a triple monochromator, a 5 mW Ar+ laser (λ = 780 nm) excitation source), (iv) X-ray photoelectron spectroscopy (XPS, a Kratos AXIS Ultra DLD instrument using a monochromatic Al Kα X-ray source at 1486.6 eV and operated at 150 W, 15 kV and 10 mA, of which high-resolution spectra (C1s and O1s) were acquired using a pass energy of 20 and 0.1 eV energy steps and all binding energies were referenced to the hydrocarbon C1s peak at 285 eV), (v) elemental analysis (EA, combustion through the PE2400 Series II, Perkin-Elmer), (vi) selected area electron diffraction analysis (SAED, JEOL JEM-2100), (vii) X-ray diffraction analysis (XRD, a Rigaku DMAX 2200/Ultima+ diffractometer using Cu Kα radiation source and operating at 40 kV and 30 mA), and (viii) thermogravitational analysis (TGA, Mettler-Toledo SDTA 8515).

Curcumin Loading. CCNs were labeled with tetramethylrhodamine-5-carbonyl azide (TAMRA) through a standard coupling reaction using carbodiimide (EDCI) and N-hydroxysuccinamide (NHS) (see the Supporting Information). To prepare curcumin-loaded CCNs, curcumin solution (4.0 mg of curcumin in 0.5 mL of ethanol) was added to an aqueous suspension of TAMRA-CCNs (10.0 mL containing 8.0 mg of TAMRA-CCNs) and the mixture was incubated at room temperature for 3 h. The suspension was dialyzed against water under light-proof conditions. The suspension was centrifugally filtered and the dialysate water was analyzed for unbound curcumin using UV−vis absorption spectrophotometry. To determine the curcumin encapsulation efficiency, the freeze-dried curcumin-loaded TAMRA-CCNs were suspended in ethanol (5.0 mL) and incubated under light-proof conditions at room temperature for 1 h. Then, the suspension was centrifugally filtered through a MWCO 100 000 membrane (Millipore Amicon Ultra-15) and the ethanol extract (elutant) was collected. The concentration of curcumin in the extract was determined by measuring the absorbance at 425 nm by UV/vis spectroscopy with reference to a curcumin standard curve.[34] The EE and curcumin loading level were calculated using eqs 1 and 2, respectively, as follows

$$\%\mathrm{EE} = 100(\mathrm{Ce}/\mathrm{Ci}) \quad (1)$$

$$\%\text{curcumin loading} = 100(\mathrm{Ce}/\mathrm{Cs}) \quad (2)$$

Where Ce, Ci, and Cs are the weights of the extracted curcumin, the curcumin initially added and curcumin-loaded particles, respectively.

Cellular Uptake of CCNs. The human embryonic kidney (HEK293T) and human epidermoid cervical carcinoma (CaSki) cell lines (purchased from ATCC, cultured as detailed in the Supporting Information), at a density of 3×10^5 cells per well, were seeded in six-well plates on coverslips and incubated overnight. The curcumin, as either free curcumin or as curcumin-loaded TAMRA-CCNs at a curcumin concentration of 8 ppm, as well as the phosphate buffered saline (PBS, 137 mM NaCl, 2.7 mM KCl, 10 mM $NaHPO_4$/NaH_2PO_4, pH 7.2) negative control, were added directly to the adhered cells in each well and incubated as above for 2 h. The cells were then washed and replaced with fresh complete medium (CM) three times (see the Supporting Information), fixed in 1.0 mL of 4.0% (w/v) paraformaldehyde for 15 min and then washed with CM. Cells were then incubated with 50 μL of 0.1 mg/mL acridine orange solution for 10 min, washed with CM and then analyzed by confocal laser scanning fluorescent microscopy (CLSFM, Nikon Digital Eclipse C1−Si equipped with Plan Apochromat VC 100×, Melles Griot Diode Laser and 85 YCA-series Laser at 405 and 561 nm, a Nikon TE2000-U microscope, a 32-channel-PMT-spectral-detector and Nikon-EZ-C1 Gold Version 3.80 software).

Assessment of Cell Viability. The assessment of cell viability was performed using the 3-(4,5-dimethylthiazol-2-yl)-2−5-diphenyltetrazolium bromide (MTT) mitochondrial activity assay as a surrogate measure of cell viability (see the Supporting Information).

RESULTS AND DISCUSSION

CCN Synthesis. When graphite was oxidized using a process from that of Hummers and Offeman,[35] with H_2SO_4/$NaNO_3$/$KMnO_4$ under sonication, various shapes of carbon nanoparticulates including sheets, tubes and spheres, as observed through SEM and TEM, were obtained in the suspension (Scheme 1). The spherical particles of ~130 nm

diameter interested us, so the exfoliation process was adjusted to maximize the yield of these spheres (the modified and optimized process is detailed in the Experimental Section), which is the focus of this report. By centrifugation, particulates of different shapes could be roughly separated from one another, and the ~130 nm diameter sized spheres could be obtained with minimal contamination from other particulates. Centrifugation at 37 100 g resulted in a suspension of spherical nanoparticles with an average diameter of 130 nm mixed with spherical nanoparticles with an average diameter of 5 nm. The 130 nm particles (CCNs) could be harvested (with still some contamination from the 5 nm particles) by centrifugation at 157 000 g. When the starting material was changed from graphite to GNP (6–8 nm thick × 5 μm wide), the 130 nm sized particles were still produced. The particles were thought to be cluster of carbon nanospheres, and so were named CCN. From seven repeats, an average yield of CCNs from graphite or GNP was 22 ± 5% (by wt).

The freeze-dried CCN preparation could be resuspended in water with the aid of sonication (40 kHz, 25 °C, 15 min), indicating that the particles neither fused together nor formed into nondispersible tight aggregates during the drying process. At the same concentration (100 ppm), the water suspension of the CCNs was transparent yellow-brownish while that of the GOShs (precipitate from the centrifugation at 37100 g, see Scheme 1) was a deeper color (Figure 1).

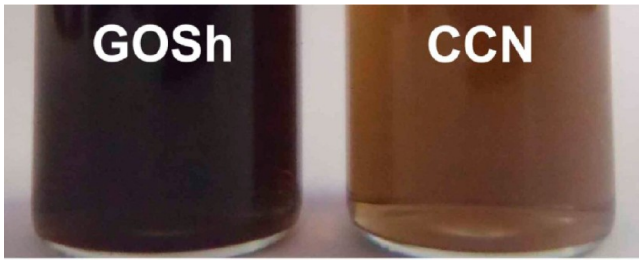

Figure 1. Images of (left) GOSh and (right) CCN suspensions, both at 100 ppm in water.

Chemical Characterization of the CCN. The UV–vis absorption spectra of the obtained CCNs and GOShs were similar with a maximum absorption at 227 nm and an extended absorption up to 600 nm (Figure 2A). The absorption profile supports the speculation of an extended π–π conjugation network. Fluorescent spectra of CCNs and GOShs were also similar, with a maximum emission at 457 nm (Figure 2B).

The ATR-FT-IR spectrum of the CCNs showed a broad OH stretching at 3344 cm^{-1}, obvious C═O stretching and C═C stretching at 1,600–1800 cm^{-1}, O–H bending and C–H bending at 1360 cm^{-1}, C–O stretching at 1205 cm^{-1}, and O–H stretching at 3300 cm^{-1} with shoulder of the C–H stretching of sp^2 carbons down to below 3000 cm^{-1} (Figure 2C), in support of the oxidized graphite in the CCNs.[36] In accordance, the Raman spectrum of the CCNs (Figure 3A) showed an obvious shoulder at 1750–1800 cm^{-1}, which indicated the C═O functionality that was absent from the Raman spectrum of graphite and is due to the oxidation of the graphite in the formation of CCN. The disorder-induced vibrational peak of the sp^2 carbon lattice, which usually appears at 1300 cm^{-1} (G band), and the peak from the stretching vibrations of the sp^2-hybridized carbon atoms, which usually appear at 1570 cm^{-1} (D band), were found to be the prominent peaks in the Raman

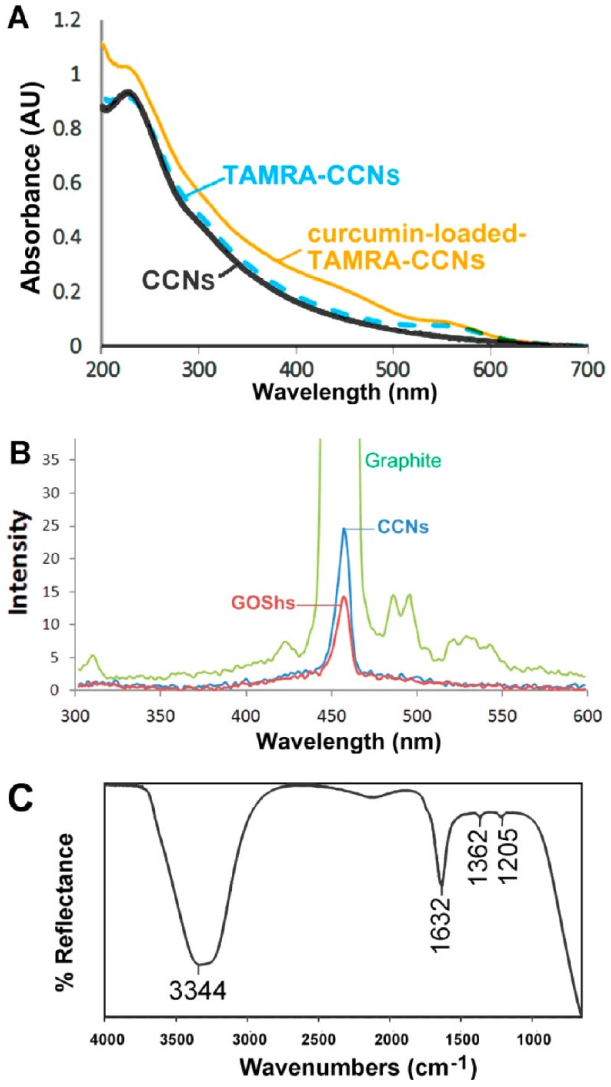

Figure 2. (A) UV absorption spectra of CCNs and TAMRA-CCNs and the curcumin-loaded TAMRA-CCNs, (B) the fluorescent spectra of CCNs, GOShs, and graphite, and (C) the FTIR spectrum of CCNs.

spectrum of CCNs. The increased D-band intensity, and the broader G and D bands, together with their slight blue shift in the CCNs spectrum compared to that of graphite, clearly indicated the structural deformation of the sp^2-hybrid carbon plane. The deformation would have resulted from the random introduction of carbonyl and hydroxyl groups into the carbon network structure during the preparation of the CCNs by the chemical exfoliation/oxidation of graphite or GNP.

X-ray photoelectron spectroscopic (XPS) analysis revealed the C–C, C═C, C–O, C═O, and COOH functional groups at the surface of the CCNs as follows. The C1s spectrum showed the binding energy (BE) of the C–C, C═C, C–O (from C–O–C and C–OH), C═O, and COOH functional groups at 283.6, 284.3, 286.3, 288.1, and 289.4 eV, respectively (Figure 3B). The O1s spectrum showed the BE of the C–O (from C–O–C and C–OH), C═O and COOH functional groups at 533.0, 531.7, and 530.5 eV, respectively (Figure 3C), confirming the oxidized carbon structure of the CCN. The C/O molar ratio deduced from XPS data, which corresponds to the composition at the surface of the materials (less than 8 nm depth) was 0.3 (see the Supporting Information), whereas the elemental analysis (EA), obtained through the combustion of

dx.doi.org/10.1021/am3019959 | ACS Appl. Mater. Interfaces 2012, 4, 6808–6815

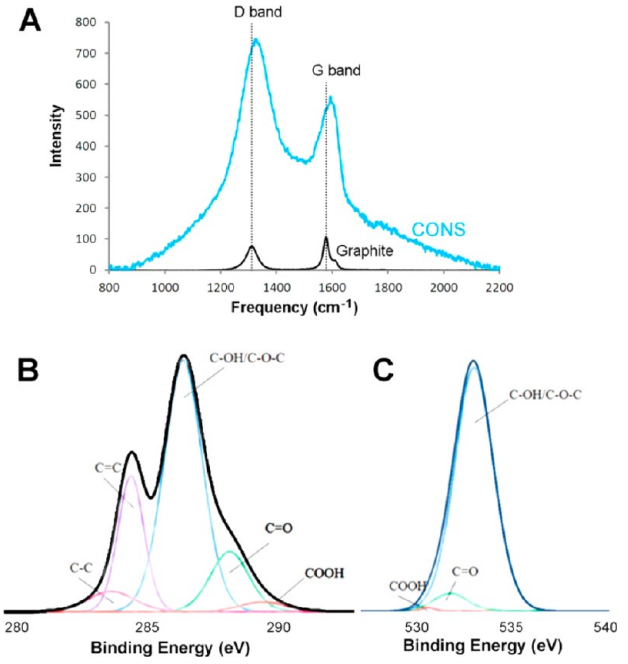

Figure 3. (A) Raman spectra of CCNs and graphite, and (B, C) the XPS derived deconvoluted (B) C1S and (C) O1S spectra of the CCNs.

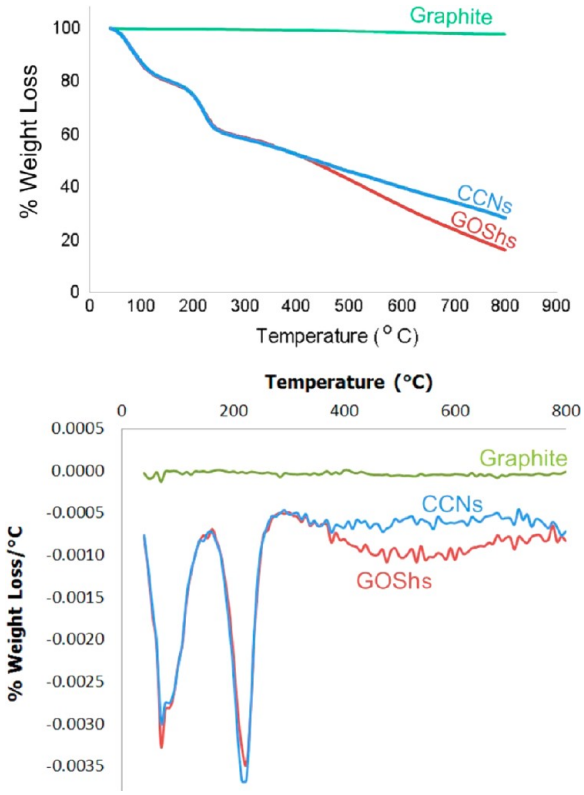

Figure 4. TGA-derived thermograms of graphite, CCN, and GOSh.

CCNs, revealed a C/O molar ratio of 1.6. This implies a more heavily oxidized carbon structure or a more hydrated nature at the particles' surface compared to that at the inside of the CCNs. However, the higher C/O atomic ratio of the CCNs obtained from the combustion analysis (1.6) is similar to that of hydrated GOShs reported earlier,[33] suggesting the discrepancy between that derived from XPS and EA analysis may lie in the hydrated state of the CCN (see thermal gravimetric analysis (TGA) analysis below). Nevertheless, the lower C/O ratios of the CCN compared to those of the two starting materials (7.4 for graphite and 12.7 for GNPs) indicates the heavily oxidized structure of the CCN, with the CCNs being only a little less oxidized than the GOShs, the latter obtained as byproduct (Scheme 1). It should be noted here that both the CCNs and the GOShs were prepared in an aqueous environment and dried under vacuum, so it is very likely that some water molecules would be trapped in the materials, giving the low C/O ratios. Indeed, in support of this notion is that the thermograms of GOShs and CCNs (Figure 4) show an initial mass loss at less than 100 °C that is attributable to absorbed water. Thereafter, a mass loss at around 200 °C, which has previously been ascribed to the decomposition of oxidized carbon functional groups,[37] and then a steady mass loss at 400−800 °C that is attributed to the sublimation and burning of the damaged graphitic materials, was seen. Compared to that for GOSh, the CCN showed a slower mass loss at 400−600 °C (Figure 4), agreeing well with the fact that GOSh possess a higher surface area than CCN.

Morphology of the CCN. SEM analysis of the dried CCNs revealed their spherical architecture with an average diameter of 129.6 ± 0.1 nm (Figure 5A) which is quite similar to the average diameter of 132.13 ± 4.74 nm (PDI of 0.388) obtained from the DLS analysis of the aqueous suspension of CCNs. Their high surface charges in water and phosphate buffer saline (zeta potentials of −47.56 ± 1.18 and −29.15 ± 1.02 mV (mean ± 1 SD) in water and phosphate buffer saline, respectively) correspond well to the stability of CCN aqueous suspension in both media.

TEM analysis of the CCNs revealed the presence of many spherical shapes with a diameter of ∼5 nm and sheet like materials inside the 130 nm CCNs (Figures 5B−C and 6A, also see more pictures in the Supporing Information), which implies that the CCN is likely to be an aggregate of many ∼5 nm spheres and sheets. The fact that CCNs could not be centrifuged down easily, rather the materials remained in the supernatant during centrifugation at 37100 g, whereas the more hydrophilic GOShs with a higher surface area were pelleted down, suggests that the small spherical substructure of CCNs might be hollow (see also Figure 5C and Figure S6 in the Supporting Information). Nevertheless, this has to be further elucidated.

The two turbostratic graphite derived starting materials, natural flake graphite and GNPs, gave CCNs of the same particle size. Thus, interestingly, when GNPs of only 6−8 nm thick were used as the starting material, the CCNs with a diameter of ∼130 nm could still be synthesized, and so in this case the CCN had to be assembled from smaller pieces. The mechanism for the formation of CCN is unknown for certain, but we speculate that one possibility is as follows. During the exfoliation/oxidation of graphitic materials, various nanosized particulates, including hollow spherical carbon particles (giant fullerene balls) together with graphene sheets and GOShs, were generated and, due to their hydrophobic surfaces, quickly aggregated. Since the oxidizing agents were present in high concentration (higher than those used in Hummer and Offeman process,[35] as optimized for the maximum CCN yield), oxidation of these carbon particles took place at the same time as their aggregation. The outer part of the CCN particle, therefore, was oxidized more than the protected

dx.doi.org/10.1021/am3019959 | ACS Appl. Mater. Interfaces 2012, 4, 6808−6815

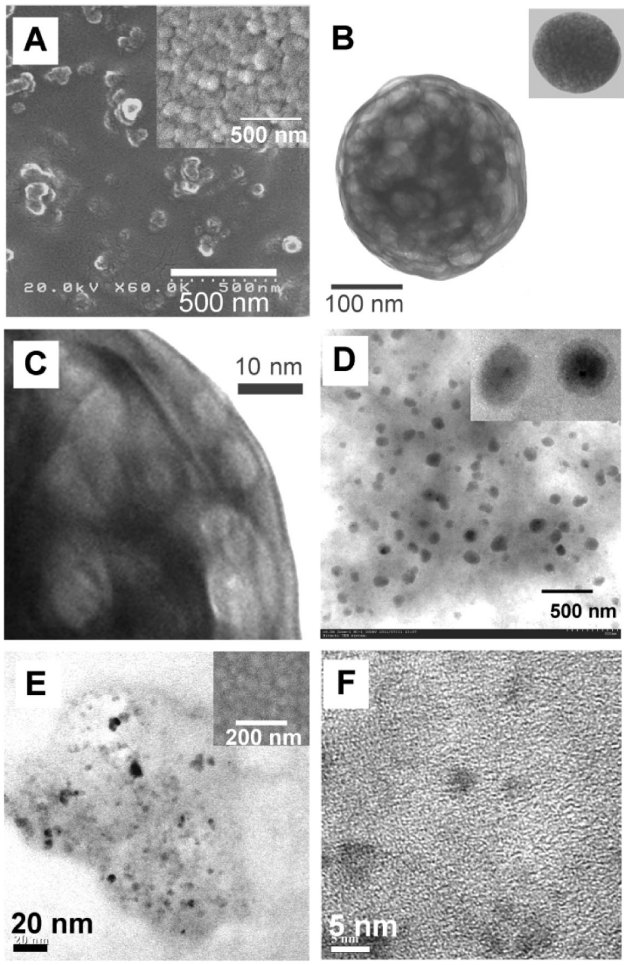

Figure 5. Representative (A) (and inset of E) SEM and (B–F) TEM images of (A–C) CCNs, (D) curcumin-loaded-TAMRA-CCNs, and (E, F) the small nanospheres which were partially separated from CCNs as the supernatant after the 157 000 g centrifugation. Image C is the expansion of B. Insets in A and B show a different view of the same sample type, whereas the inset of D is its expansion.

hydrophobic inner core of the particles until the surface oxidation level was enough to produce stable CCNs with a high enough zeta potential (−47.56 ± 1.18 mV) to repel further attachment of any more particles, and so their growth stopped. TEM images of CCN (Figure 5B–C and 6A) support this mechanism as many small particles (diameter of ∼5 nm) and some sheetlike materials could be observed inside each CCN. As discussed earlier, both the 5 nm spheres and the GOShs were also being produced and detected in the reaction mixture. The GOShs could be centrifuged down easily (P1 of Scheme 1), while the 5 nm spheres were abundantly left in the supernatant during the CCNs separation (S2 of Scheme 1) (see Figure 5E-F and also Figure S4 and S5 in the Supporting Information). The size of these spheres is similar to those observed inside the CCNs. The presence of these particles in the reaction mixture supports the proposed mechanism for CCN formation. The possibility that CCNs are composed of many giant fullerene and GOShs is further supported by the observed selected area electron diffraction (SAED) patterns of the CCN. The SAED patterns obtained from CCN show several sets of smeared and diffuse diffraction spots, indicating that the material is neither entirely single crystalline nor amorphous (Figure 6, see also the SAED patterns of graphite

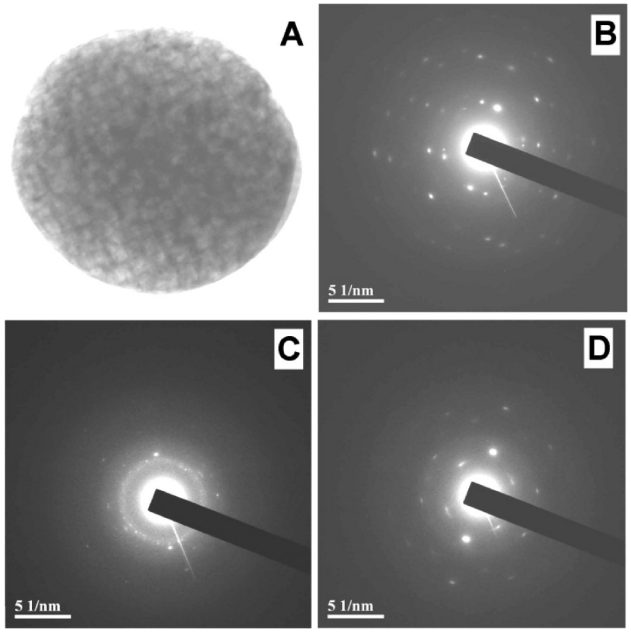

Figure 6. (A) CCN, with (B–D) the selected area electron diffraction (SAED) patterns obtained from three different areas.

and GNP in the Supporting Information). The XRD pattern of the CCN compared to that of the GNPs (see the Supporting Information) also indicated the reduced crystallinity of the material. To the best of our knowledge, CCNs have never been experimentally detected before, but their structure resembles those theoretically predicted and studied by Grimme et al.[38]

At present, there is no solid explanation as to how the 5 nm spheres are formed. However, reasonable explanations can be deduced from previous research work as follows. The first plausible explanation is that the GOShs generated in the reaction mixture disintegrated into polyaromatic hydrocarbon (PAH) pieces and the generated PAHs then assembled into giant oxidized fullerenes. This explanation is actually based on the report of Wang et al.,[28] which demonstrated that in solution under sonication, GOShs could disintegrate into PAHs and the generated PAHs could assemble into fullerene and CNTs. The other plausible explanation is that the giant fullerene could directly be generated from GOShs during the sonication process. This explanation is based on the report of Chuvilin et al. who demonstrated that fullerenes could be produced directly from graphene sheets through the reaction of carbons at the edge of carbon network sheets.[29]

Curcumin Loading. To follow CCNs within cells, we covalently linked the fluorophore TAMRA to the CCNs to obtain TAMRA-CCNs. Successful grafting was confirmed by the appearance of a new small absorption band at 565 nm in the UV–vis absorption spectrum of TAMRA-CCNs (Figure 2A) and also the obvious fluorescent nature of the TAMRA-CCNs under the fluorescent microscope (data not shown, but see Figure 7D-G). Thus, the fluorescent labeled TAMRA-CCNs could be used to monitor their uptake (probably by endocytosis) into living cells together with their distribution (once internalized) within the cells by confocal laser scanning fluorescent microscope (CLSFM).

Curcumin (1,7-bis(4-hydroxy-3-methoxyphenyl)-1,6-heptadiene-3,5-dione) is a recognized pharmaceutically safe yellow pigment that is isolated from the rhizomes of the turmeric plant (*Curcuma longa* L.). The various biological activities of this

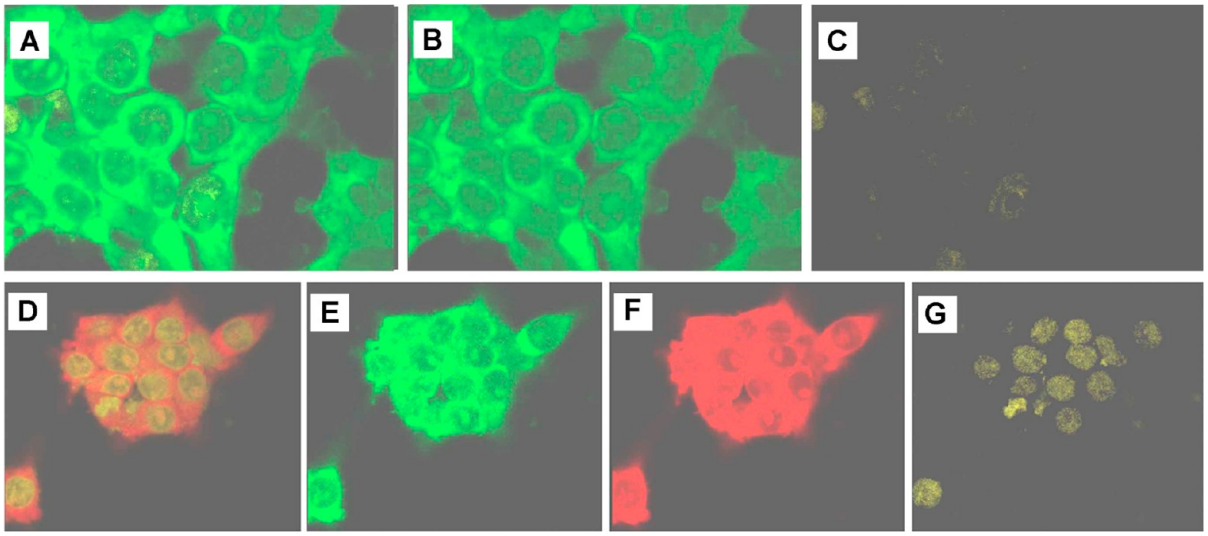

Figure 7. Multiple stain confocal images of HEK293T cells after being incubated with (A−C) free curcumin, or (D−G) curcumin-loaded TAMRA-CCNs, for 2 h at 37 °C under 5% (v/v) CO2. Images are the (A, D) original or the (B, C, E−G) color separated, and show the fluorescence signal from curcumin in yellow, that from TAMRA in red, and that from acridine orange in green. The concentration of curcumin was (A−C) 0.74 μg/mL and (D−G) 0.74 μg/mL with CCNs at 3.26 μg/mL, and the cell density was 3×10^5 cells/well in all cases.

compound have been well documented, including an anticancer activity.[39] Curcumin, however, is easily degraded and possesses a poor bioavailability,[40] due largely to its water insolubility and fast blood clearance characteristics. Since the structure of curcumin contains an extensive $\pi-\pi$ conjugation with two aromatic moieties, the compound should easily attach non-covalently to the CCN surface via $\pi-\pi$ stacking, making curcumin a potentially suitable compound as a cargo to test the CCNs as a delivery material. In addition, in contrast to most potent anticancer drugs, curcumin emits a strong fluorescent signal at the λ_{max} of 530 nm, and so the use of CLSFM to monitor its location inside the living cells is possible. Here, the curcumin loading on TAMRA-CCNs of 18.5 ± 1.4% (w/w of curcumin to curcumin-loaded CCNs), as analyzed by directly extracting curcumin from the CCNs and by quantifying curcumin in the extract, was achieved. The adsorption of curcumin on CCNs is likely to be a result of the $\pi-\pi$ stacking interaction between the $\pi-\pi$ conjugation network of curcumin molecules and that of the CCN, similar to the absorption of molecules with aromatic substructures on GOShs reported previously.[41] The UV−vis absorption spectrum of the water suspension of the resulting curcumin-loaded TAMRA-CCNs showed similar absorption pattern to that of the CCNs but with shoulder peaks at 430 nm from curcumin and 565 nm from TAMRA (Figure 2A), confirming the presence of curcumin on the TAMRA-CCNs. Inspection of the suspension by optical microscopy revealed no evidence of any curcumin precipitate. TEM analysis of the curcumin-loaded CCNs revealed a similar spherical structure to the unloaded CCNs and the TAMRA-CCNs (Figure 5D).

Cellular Uptake of Curcumin-Loaded TAMRA-CCN. After HEK293T cells were incubated with TAMRA-CCNs for 2 h under standard culture conditions, and then thoroughly washed, stained with acridine orange and subjected to CLSFM analysis, the fluorescence signal of the grafted TAMRA could clearly be detected in the cytoplasm of the cells. It was concluded that the TAMRA-CCNs could be taken up by the cells. Moreover, the TAMRA-CCNs remained localized within small cytoplasmic compartments and did not gain entry into the nucleus. When the HEK293T cells were incubated with the curcumin-loaded TAMRA-CCNs under otherwise identical conditions, a clear fluorescence signal from both curcumin and TAMRA could be observed inside the cells but at different locations (Figure 7D−G). The curcumin fluorescence (yellow) was observed in the nucleus (Figure 7G), whereas that from TAMRA (red) was only found in the cytoplasm (Figure 7F). This implies that curcumin dissociated from the TAMRA-CCN carriers once inside the cells and then entered the nucleus. Compared to that obtained when free curcumin at the same concentration was incubated with the cells, it was obvious that without the CCN carriers, the uptake of curcumin into the cells was dramatically reduced (Figure 7A−C).

In vitro Cytotoxicity of CCN. The cell viability was assayed to estimate the toxicity of CCNs by the MTT method as a surrogate cell viability assay. When the HEK293T and human epidermoid cervical carcinoma (CaSki) cells were cultured in vitro with the CCN at concentrations of 0.01−1.0 μg/mL they showed no signs of cytotoxicity, with cell viabilities of 102% and 90%, respectively, as determined by the MTT cell cytotoxicity assay (Figure 8). The relatively low in vitro cytotoxicity of the CCNs indicated the biocompatibility of CCNs, at least in vitro

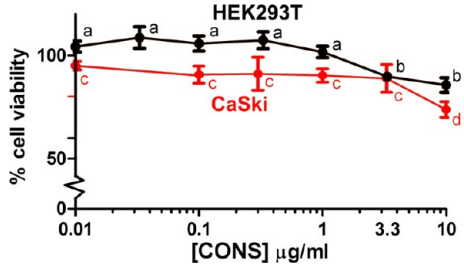

Figure 8. In vitro cytotoxicity of various concentrations of CCNs or curcumin-loaded CCN (18.5 ± 1.4% (w/w) curcumin loading) compared to that for free curcumin (at the same ppm curcumin as the loaded CCN) on the HEK293T and CaSki cells after a 48 h exposure. Data are shown as the mean ±1 SD and are derived from three independent repeats.

at concentrations of <3.3 μg/mL (see Figure 8). In contrast, the curcumin-loaded CCN lead to a 2.5-fold greater reduction in the cancer cell viability than that obtained with free curcumin alone at the same level. Thus, the potential to use CCNs as a delivery vehicle for high potency anticancer drugs, such as paclitaxel, is under evaluation.

CONCLUSION

A new nanoarchitectural form of carbon network-based material, CCN of approximately 130 nm diameter spheres, were synthesized through a sonication assisted oxidation/exfoliation of graphite or GNPs, and then centrifugally separated from other nanostructures. TEM analysis revealed that the CCN were likely to be composed of an aggregate of 5 nm hollow particles (giant fullerenes) and GOShs. Although CCN is first reported here, its structure resembles the theoretically studied carbon nanostructure presented earlier.[37] CCN appears to be able to be used as an effective drug carrier and offers (i) a 19% (w/w) loading of curcumin, a hydrophobic drug with a π conjugation substructure, (ii) the ability to be taken up into the cells, probably by endocytosis, (iii) the ability to release the loaded curcumin once inside the cells, (iv) noninvasiveness of the CCNs to the nucleus, and (v) a low cytotoxicity when used at <3.3 μg/mL.

ASSOCIATED CONTENT

Supporting Information

Experimental details on coupling of TAMRA to CCNs, cell culture, and toxicity assessment; SAED patterns of graphite and GNPs; XRD patterns of graphite, GNP, CCN, and GOSh. This material is available free of charge via the Internet at http://pubs.acs.org.

AUTHOR INFORMATION

Corresponding Author

*Tel: (662) 218-7634. Fax: (662) 254-1309. E-mail: psupason@chula.ac.th.

Funding

This study is financially supported by the Thailand Research Fund (BRG grant), the Special Task force for Activating Research (STAR) from the Centenary Academic Development Project, Chulalongkorn University and the Program of Center of Excellence Network from Nanotechnology Center (NANOTEC), NSTDA, Ministry of Science and Technology, Thailand.

Notes

The authors declare no competing financial interest.

ABBREVIATIONS

CCNs, cluster of carbon nanospheres; GNP, graphene nanoplatelet

REFERENCES

(1) Kroto, H. W.; Heath, J. R.; O'Brien, S. C.; Curl, R. F.; Smalley, R. E. *Nature* **1985**, *318*, 162.
(2) Smalley, R. E. *Acc. Chem. Res.* **1992**, *25*, 98.
(3) Rietmeijer, F. J. M.; Rotundi, A.; Heymann, D. *Fullerenes, Nanotubes, Carbon Nanostruct.* **2004**, *12*, 659.
(4) Iijima, S.; Ajayan, P. M.; Ichihashi, T. *Phys. Rev. Lett.* **1992**, *69*, 3100.
(5) Ugarte, D. *Nature* **1992**, *359*, 707.
(6) Kasuya, D.; Yudasaka, M.; Takahashi, K.; Kokai, F.; Iijima, S. J. *Phys. Chem. B* **2002**, *106*, 4947.
(7) Muszynski, R.; Seger, B.; Kamat, P. V. *J. Phys. Chem. C* **2008**, *112*, 5263.
(8) Xu, Y.; Liu, Z.; Zhang, X.; Wang, Y.; Tian, J.; Huang, Y.; Ma, Y.; Zhang, X.; Chen, Y. *Adv. Mater.* **2009**, *21*, 1275.
(9) Yoshitake, T.; Shimakawa, Y.; Kuroshima, S.; Kimura, H.; Ichihashi, T.; Kubo, Y.; Kasuya, D.; Takahashi, K.; Kokai, F.; Yudasaka, M.; Iijima, S. *Physica B* **2002**, *323*, 124.
(10) Ni, G.-X.; Zheng, Y.; Bae, S.; Tan, C. Y.; Kahya, O.; Wu, J.; Hong, B. H.; Yao, K.; Özyilmaz, B. *ACS Nano* **2012**, *6*, 3935.
(11) Xu, L. R.; Bhamidipati, V.; Zhong, W.-H.; Li, J.; Lukehart, C. M.; Lara-Curzio, E.; Liu, K. C.; Lance, M. J. *Compos. Mater.* **2004**, *38*, 1563.
(12) Liu, Y.; Yu, D.; Zeng, C.; Miao, Z.; Dai, L. *Langmuir* **2010**, *26*, 6158.
(13) Wang, X.; Zhi, L.; Tsao, N.; Tomović, Ž.; Li, J.; Müllen, K. *Angew. Chem.* **2008**, *120*, 3032.
(14) Kim, J.; Cote, L. J.; Kim, F.; Yuan, W.; Shull, K. R.; Huang, J. *J. Am. Chem. Soc.* **2010**, *132*, 8180.
(15) Bekyarova, E.; Murata, K.; Yudasaka, M.; Kasuya, D.; Iijima, S.; Tanaka, H.; Kahoh, H.; Kaneko, K. *J. Phys. Chem. B* **2003**, *107*, 4681.
(16) Hu, W.; Peng, C.; Luo, W.; Lv, M.; Li, X.; Li, D.; Huang, Q.; Fan, C. *ACS Nano* **2010**, *4*, 4317.
(17) Wick, P.; Manser, P.; Limbach, L. K.; Dettlaff-Weglikowska, U.; Krumeich, F.; Roth, S.; Stark, W. J.; Bruininck, A. *Toxicol. Lett.* **2007**, *168*, 121.
(18) Zhang, L.; Lu, Z.; Zhao, Q.; Huang, J.; Shen, H.; Zhang, Z. *Carbon* **2011**, *49*, 986−995.
(19) Heister, E.; Neves, V.; Tîlmaciu, C.; Lipert, K.; Beltrán, V. S.; Coley, H. M.; Silva, S. R. P.; McFadden, J. *Carbon* **2009**, *47*, 2152−2160.
(20) Lacerda, L.; Pastorin, G.; Gathercole, D.; Buddle, J.; Prato, M.; Bianco, A.; Kostarelos, K. *Adv. Mater.* **2007**, *19*, 1480−1484.
(21) Liu, Z.; Chen, K.; Davis, C.; Sherlock, S.; Cao, Q.; Chen, X.; Dai, H. *Cancer Res.* **2008**, *68*, 6652.
(22) Yang, X.; Zhang, X.; Liu, Z.; Ma, Y.; Huang, Y.; Chen, Y. *J. Phys. Chem. C* **2008**, *112*, 17554.
(23) Zhang, L.; Lu, Z.; Zhao, Q.; Huang, J.; Shen, H.; Zhang, Z. *Small* **2011**, *7*, 460.
(24) Zhang, L.; Xia, J.; Zhao, Q.; Liu, L.; Zhang, Z. *Small* **2010**, *6*, 537.
(25) Shi, X.; Sitharaman, B.; Pham, Q. P.; Liang, F.; Wu, K.; Edward Billups, W.; Wilson, L. J.; Mikos, A. G. *Biomaterials* **2007**, *28*, 4078.
(26) Zanello, L. P.; Zhao, B.; Hu, H.; Haddon, R. C. *Nano Lett.* **2006**, *6*, 562.
(27) Sun, X.; Liu, Z.; Welsherxxx, K.; Robinson, J.; Goodwin, A.; Zaric, S.; Dai, H. *Nano Res.* **2008**, *1*, 203.
(28) Wang, S.; Tang, L. A. l.; Bao, Q.; Lin, M.; Deng, S.; Goh, B. M.; Loh, K. P. *J. Am. Chem. Soc.* **2009**, *131*, 16832.
(29) Chuvilin, A.; Kaiser, U.; Bichoutskaia, E.; Besley, N. A.; Khlobystov, A. N. *Nat. Chem.* **2010**, *2*, 450.
(30) Kosynkin, D. V.; Higginbotham, A. L.; Sinitskii, A.; Lomeda, J. R.; Dimiev, A.; Price, B. K.; Tour, J. M. *Nature* **2009**, *458*, 872.
(31) Yuge, R.; Yudasaka, M.; Toyama, K.; Yamaguchi, T.; Iijima, S.; Manako, T. *Carbon* **2012**, *50*, 1925.
(32) Zhu, S.; Xu, G. *Nanoscale* **2010**, *2*, 2538.
(33) Park, S.; Ruoff, R. S. *Nat. Nanotechnol.* **2009**, *4*, 217.
(34) Suwannateep, N.; Banlunara, W.; Wanichwecharungruang, S. P.; Chiablaem, K.; Lirdprapamongkol, K.; Svasti, J. *J. Controlled Release* **2011**, *151*, 176.
(35) Hummers, W. S.; Offeman, R. E. *J. Am. Chem. Soc.* **1958**, *80*, 1339.
(36) Oh, W. C.; Zhang, F. J. *Asian J. Chem.* **2011**, *23*, 875.
(37) Jeong, H. K.; Lee, Y. P.; Jin, M. H.; Kim, E. S.; Bae, J. J.; Lee, Y. H. *Chem. Phys. Lett.* **2009**, *470*, 255.
(38) Grimme, S.; Mück-Lichtenfeld, C.; Antony, J. *J. Phys. Chem. C* **2007**, *111*, 11199.
(39) Sharma, R. A.; McLelland, H. R.; Hill, K. A.; Ireson, C. R.; Euden, S. A.; Manson, M. M.; Pirmohamed, M.; Marnett, L. J.; Gescher, A. J.; Steward, W. P. *Clin. Cancer Res.* **2001**, *7*, 1894.

(40) Tonnesen, H. H.; Karlsen, J.; van Henegouwen, G. B. *Z. Lebensmitt Unters. Forsch.* **1986**, *183*, 116.
(41) Liu, Z.; Robinson, J. T.; Sun, X.; Dai, H. *J. Am. Chem. Soc.* **2008**, *130*, 10876.